Initiation and Polymer Density of Conjugated Polymer Brushes

Ian A. VonWald, S. Gaither Frye, Mark M. Moog, Carrie L. Donley, Frank Tsui,* and Wei You*

ABSTRACT: The growth mechanism and polymer density in conjugated polymer brush (CPB) films composed of poly(3-methylthiophene) (P3MT) are characterized. X-ray photoelectron spectroscopy experiments show that the initiation of aryl halide monolayers by $Pd(P^tBu_3)_2$ produces disproportionated monolayer initiators. Unlike disproportionated species formed during the solution-phase initiation of aryl halides, which cannot mediate polymerization, the surface-bound initiators catalyze polymerization to form CPB films with a high grafting density (1.2 nm^{-2}). Rutherford backscattering spectrometry (RBS) experiments show that P3MT CPB films have a characteristic monomer volume density (3.7 nm^{-3}) that is indistinguishable from the volume density of spuncast poly(3-hexylthiophene) films. Using these RBS and XPS results, characteristics of P3MT CPB growth are obtained, including the turnover frequency (7.5 h^{-1}) and polymer molecular weight (300 g/mol·nm).

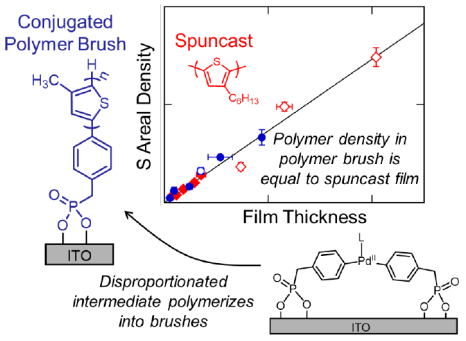

INTRODUCTION

Conjugated polymer brush (CPB) films, such as those composed of poly(3-methylthiophene) (P3MT), are a promising platform for studying intramolecular charge-transport phenomena in organic semiconductors.[1] CPBs are grown from the substrate surface, in contrast to conventionally deposited (i.e., spun-cast), presynthesized conjugated polymers. Because of this difference, CPB film properties, such as the morphology and charge transport, are different from those of spun-cast polymer films. CPB films have been found to be more vertically oriented than spun-cast films, and they potentially possess enhanced intramolecular charge-transport pathways in the vertical direction.[1] These characteristics have motivated the use of CPB films in a variety of applications, including thermoelectronics, spintronics, and solar cells.[2−4]

Despite these advances in the characterization and application of CPBs, there are many important properties of the material that are unknown, such as the mechanism of CPB growth and various pertinent physical properties, including the grafting density (i.e., the number of tethered polymer chains per unit area), polymer density (i.e., the density of repeat units per unit volume in the film), molecular weight (i.e., the number-average molecular weight of tethered polymers), and charge mobility. These properties must be understood in order to effectively use CPBs to study intrinsic charge-transport phenomena and for technological applications.

The mechanism of conjugated polymer growth in solution is well known, including the chemical species resulting from polymerization or disproportionation, which have been thoroughly characterized using standard synthesis techniques (e.g., NMR and XRD).[5,6] In contrast, there has been limited attention in the literature on characterizing the chemical structure or density of species present during the initiation of surface-bound monolayers (MLs) with metal catalysts (elsewhere called initiators but referred to here as initiated MLs) and the subsequent polymerization of CPBs.[7−9] The chemical structure and density of the initiated MLs play a key role in determining important qualities of the resulting CPB films, such as the grafting density and, by extension, the polymer orientation.[10] However, many reports that characterize CPB films assume that the species responsible for the initiation and polymerization of CPBs are identical to the analogous processes in solution, without providing experimental evidence for the chemical species on the surface to support this assertion.[8,9,11]

The polymer density and molecular weight are important properties of conjugated polymer films that can influence other film characteristics, such as the structure, morphology, and charge transport.[12−16] Unfortunately, these quantities are difficult to measure in CPB owing to the insolubility of the polymer (i.e., P3MT). Similarly, charge-transport properties of CPBs, such as charge mobility, have not been thoroughly characterized, owing primarily to the complexity and heterogeneity of electrical contacts, contact potentials, and interfacial states present in the devices made from these films. Because of these difficulties, while CPB films have been shown to exhibit reduced resistivity compared to spun-cast films, the

Received: July 28, 2020
Revised: September 22, 2020
Published: October 15, 2020

cause of the observed reduction is still unknown (i.e., whether it originates from a difference in carrier mobility, carrier concentration, other effects, or a combination of these).[1]

Here, we used X-ray photoelectron spectroscopy (XPS) and Rutherford backscattering spectrometry (RBS) to further investigate CPB growth and film properties. Specifically, XPS was used to characterize the chemical structure and density of species present during initiation. We found that disproportionated MLs are formed during initiation, which would be expected to preclude chain propagation in solution-phase conjugated polymer synthesis. Interestingly, we find that these disproportionated MLs are actually responsible for catalyzing dense CPB growth with a Pd catalyst. RBS was used to measure the polymer density in CPB films, which have a constant volume density regardless of film thickness. Additionally, the volume density in CPB films was found to be equal to the volume density of analogous spun-cast polymer films. XPS and RBS results were combined to produce important parameters of CPB growth, including the molecular weight and turnover frequency. These findings improve our understanding of the growth, morphology, and charge transport in CPB films and provide the impetus for further exploring these phenomena and ultimately controlling them in the future.

EXPERIMENTAL SECTION

Materials. All chemicals and reagents were purchased from commercial sources (Sigma-Aldrich, Acros, Strem, etc.) and used without further purification unless otherwise noted. Dry THF was purified by distillation, and dry toluene (Fisher Chemicals) was used without further purification. Soda-lime glass slides (1 in. × 1 in.) with a 145-nm-thick sputtered indium tin oxide (ITO) layer and fused quartz slides with a 60- or 32-nm-thick sputtered ITO layer were purchased from Thin Film Devices, Inc. The roughnesses of the 145-, 60-, and 32-nm-thick ITO films were 0.3, 0.4, and 0.1 nm, respectively, and the sheet resistivity was 20 Ω/sq for all ITO films. The ITO glass slides were used for initiation characterization experiments, while the ITO quartz slides were preferred for RBS experiments to enhance the sensitivity for detecting and quantifying the chemical species within the polymer films (see below).

Monolayer Formation. ITO slides were cleaned and functionalized with pristine monolayers (MLs) of (4-bromophenyl)phosphonic acid (**ML-Br**) or (4-iodophenyl)phosphonic acid (**ML-I**) using a method described previously.[1]

Monolayer Initiation. ITO slides functionalized with pristine **ML-Br** or **ML-I** were immersed in a solution of the catalyst without stirring in an oxygen- and water-free glovebox. After exposure to the catalyst, initiated ML films were rinsed extensively with toluene and THF and transferred immediately to XPS analysis or derivatization without exposure to air.

For initiation using $Pd(P^tBu_3)_2$, 51 mg of the catalyst (Strem Chemicals, 0.1 mmol) was dissolved in toluene (10 mL, 10 mM solution). The monolayer-functionalized ITO slides were added and left for 3 h at 70 °C.[1,9]

For initiation using Ni(dppp) (dppp = bis(diphenylphosphino)propane), 2,2′-bipyridine (bpy, 39.8 mg, 0.25 mmol) and $Ni(COD)_2$ (COD = 1,5-cyclooctadiene) (70 mg, 0.25 mmol) were added to toluene (10 mL, 25 mM solution) and shaken vigorously for 1 min. The solution turned dark violet. Monolayer-functionalized ITO slides were immersed in the solution overnight at room temperature. The slides were then rinsed with just toluene and immersed in a solution of dppp (105 mg, 0.25 mmol) in toluene (10 mL, 0.025 M) overnight at room temperature for *in situ* ligand exchange from bpy to dppp.[8]

Monolayer Derivatization. For the derivatization of initiated ML slides with a thiophene functional group, commercially available bromothiophene (97 mg, 0.59 mmol) in THF (10 mL) was cooled to 0 °C. Isopropylmagnesium chloride (0.27 mL, 2 M in THF, 0.54 mmol) was added dropwise while stirring, yielding a 50 mM solution of the Grignard derivatization reagent. This solution was stirred at 0 °C for 30 min and then at room temperature for 30 min. Initiated ML films were immersed in this solution overnight at 40 °C without stirring. The resulting derivatized ML slides were rinsed with toluene and THF in the glovebox, quenched in methanol, and then cleaned outside of the glovebox in the ambient atmosphere by sonication in water, chloroform, and isopropyl alcohol for 30 s each.

For derivatization with the ferrocene functional group, 2-ferrocenyl-5-bromothiophene was synthesized according to a literature procedure.[8] This compound (177 mg, 0.67 mmol) was dissolved in THF (30 mL) and cooled to 0 °C. Isopropylmagnesium chloride (0.3 mL, 2 M in THF, 0.6 mmol) was added dropwise while stirring, yielding a 20 mM solution of the Grignard derivatization reagent. Initiated ML films were immersed in this solution and cleaned according to the same procedure as used with derivatization using bromothiophene.

Synthesis of CPB Films. Poly(3-methylthiophene) (P3MT) CPB films were grown by surface initiated Kumada catalyst transfer polycondensation (SI-KCTP).[1,9] Briefly, pristine ML films of **ML-Br** on 145-, 60-, or 32-nm-thick ITO slides were initiated using $Pd(P^tBu_3)_2$ following the method described above. The initiated ML films were rinsed thoroughly with toluene and THF and then immersed in a 0.15 M solution of the magnesiated 2-bromo-3-methyl-5-iodothiophene Grignard monomer in dry THF at 40 °C without stirring. At the desired time intervals ranging from 30 s to 32 h (with longer growth times corresponding to thicker CPB films), slides were removed from the solution and rinsed in toluene and THF. The slides were then taken out of the glovebox and sonicated in chloroform, water, and isopropanol for 30 s each. The resulting P3MT CPB films were stored in the dark under an inert atmosphere and used for subsequent experiments within a week to avoid degradation in ambient oxygen or light.

Preparation of Spun-Cast P3HT Films. Regioregular P3HT (Rieke Metals, M_n = 20 kg/mol, $Đ$ = 2.24, 86% HT) was spun cast at various speeds (300−3000 rpm) from chlorobenzene solutions of the appropriate concentrations (3−15 mg/mL) onto cleaned ITO slides. The spun-cast films were stored in the dark under an inert atmosphere and characterized without annealing within a week.

Cyclic Voltammetry (CV). CV was performed using a previously described method.[1] The grafting density d of ferrocene-derivatized ML films on ITO was calculated using the Randles−Sevcik equation[17]

$$d = \frac{4iRT}{n^2F^2\nu A} \quad (1)$$

where i is the oxidation or reduction peak area, R is the gas constant, T is the temperature, n is the number of electrons transferred, F is Faraday's constant, ν is the scan rate, and A is

the working electrode area. Using i = 75 μA (from the oxidation peak of Figure S5a), n = 1 (Fe^{2+} to Fe^{3+}), F = 9.65 × 10^4 C/mol, R = 8.314 J/K·mol, T = 298 K, ν = 0.1 V/s, and A = 3.75 cm^2, d was calculated to be 2.1 × 10^{-10} mol/cm^2 or 1.3 nm^{-2}.

X-ray Photoelectron Spectroscopy (XPS). A Kratos Axis Ultra Delay-Line Detector spectrometer was used for XPS analysis. The air-sensitive initiated ML films were loaded under dry N_2 conditions, while the less-air-sensitive samples (i.e., pristine and derivatized ML films) were loaded under an ambient atmosphere. The samples were then held under a high vacuum (ca. 7 × 10^{-9} Torr) for analysis. The X-ray source was a monochromatic Al Kα source (1486.6 eV). Samples were analyzed without a charge neutralizer. The energy of the XPS spectra was corrected to the carbon 1s peak for adventitious carbon (binding energy = 284.6 eV). The doublet peak spacing, relative intensities, atomic sensitivity factors, and general species binding energies were assigned using the Kratos software and other standard tabulated sources.[18] All background and peak fitting analysis was done with Kratos Vision software. Shirley backgrounds were applied when appropriate; otherwise, linear backgrounds were applied.

The qualitative chemical structures and densities of species in pristine, initiated, and derivatized ML films were analyzed during high-resolution XPS measurements that used a pass energy of 20 eV, an energy step of 100 mV, and dwell times ranging from 400 to 3200 ms. Peak positions and atomic concentrations are given in Table S1. The quantitative measurements of density for surface species present in pristine and thiophene-derivatized ML films were adapted from a previous report.[19] These measurements used a pass energy of 80 eV and an energy step of 100 mV, with dwell times of 400 ms for Au 4f, 3200 ms for Br 3d and S 2p, and 1600 ms for I 3d. A gold foil reference sample (Alfa Aesar, density = 19.2 g/cm^3) was sputtered with an Ar^+ ion gun in the XPS chamber for 10−15 min to remove adventitious carbon and then measured before and after the ML samples. ML samples were measured at least three times at different spots to avoid beam damage to the ML film from the X-ray. Initiated ML films were not analyzed using the quantitative XPS procedure due to the physisorption of catalyst species during initiation, which could not be cleaned off prior to XPS measurements. These catalyst species were cleaned off after ML derivatization by sonication of the films in various solvents, as described above.

The densities of atoms characterized by quantitative XPS measurements were calculated using a set of standard XPS equations and assumptions.[19−21] The areal density D of a terminal atom in a ML using Br 3d as an example analyte atomic orbital is given by

$$D_{\mathrm{Br\ 3d}} = \frac{\Gamma_{\mathrm{Br\ 3d}} s_{\mathrm{Au\ 4f}} P_{\mathrm{Au\ 4f}} L_{\mathrm{Au\ 4f}} \rho_{\mathrm{Au}} f_{\mathrm{Au}} \lambda_{\mathrm{Au}} t_{\mathrm{Au\ 4f}} \cos\xi}{\Gamma_{\mathrm{Au\ 4f}} s_{\mathrm{Br\ 3d}} P_{\mathrm{Br\ 3d}} L_{\mathrm{Br\ 3d}} f_{\mathrm{Br}} t_{\mathrm{Br\ 3d}}} \quad (2)$$

where Γ is the peak area of the quantitative XPS scan for either the reference (Au 4f) or the analyte (Br 3d, S 2p, or I 3d), s is the combined Scofield scattering cross-section of the doublet peaks (i.e., Au $4f_{5/2}$ and $4f_{7/2}$, Br $3d_{3/2}$ and $3d_{5/2}$, S $2p_{1/2}$ and $2p_{3/2}$, I $3d_{3/2}$ and $3d_{5/2}$,),[22] P is the correction parameter for reduction in photoelectron intensity due to elastic scattering,[23] L is a function of asymmetry parameter β or β_{eff} for the analyte orbital,[23,24] ρ_{Au} is the density of the gold foil reference sample (58.7 atoms/nm^3), f is the fraction of electrons in the main peak for the orbital of interest,[25] λ is the inelastic mean free path of electrons emitted from Au 4f orbitals (~1.6 nm),[26−28] t is the scan or dwell time, and ξ is the angle of emission (detector angle away from sample normal) (ξ = 0°). P = 1 is assumed for terminal atoms, where elastic scattering is ignored. L is given by

$$L = \frac{1 - \beta(3\cos^2\psi - 1)/4}{4\pi} \quad (3)$$

where β_{eff} was used instead of β for Au 4f and ψ is the angle between the incident beam and detector (60°). Peak areas were measured in counts per second, accounting for Γ/t in eq 2. Element- and orbital-specific constants are shown in Table S2. Representative high-resolution and quantitative XPS peak intensities for pristine and derivatized ML films are shown in Table S3.

Atomic Force Microscopy (AFM). CPB and the spun-cast polymer film thickness and morphology were characterized by AFM scratch profilometry and surface topography measurements, as described previously.[1]

Rutherford Backscattering Spectrometry (RBS) Experiments and Analysis. RBS experiments were performed at the tandem Van der Graff accelerator at the Triangle University Nuclear Laboratory (TUNL) using a 2 MeV $^4He^{2+}$ beam at normal incidence with respect to the sample surface. The beam was collimated to a typical size of 2.5 mm × 2.5 mm. Scattered particles were analyzed using a solid-state silicon detector with an incident solid angle of about 0.8 msr, positioned at a scattering angle of 165.2°. Typical RBS samples were cut to about 1 cm × 1 cm and mounted with metal clips on the sample target rod. Multiple spectra were acquired at an interval of roughly 5 × 10^{13} counts of incident He (roughly 10 min) in order to probe for potential beam damage. Approximately 2 × 10^{14} total counts of incident He were detected for each sample to ensure sufficient measurement statistics.

The RBS spectra were analyzed for elemental areal density versus depth (i.e., compositional depth profile). Simulations of the spectra were performed using commercial software, SIMNRA v7.01. While the simulations can generally reproduce the spectroscopic features, they often cannot accurately fit the features from the polymer films due to the films' heterogeneous, rough, and porous nature. Therefore, the integrated intensity (I_0) of a given element within each spectrum was obtained by either numerical integration or peak fitting, which was then used to determine the areal density (N). The parameters determined from this analysis were then resimulated to check for analysis accuracy.

In the center of mass frame for normal incidence, the areal density is given in terms of I_0 by[29,30]

$$N = \frac{I_0}{\left(\frac{\mathrm{d}\sigma}{\mathrm{d}\Omega}\right) Q\,\Omega} \quad (4)$$

Here, Q is the number of incident particles, Ω is the solid angle of the detector, and $\mathrm{d}\sigma/\mathrm{d}\Omega$ is the Rutherford differential scattering cross-section, given by

$$\frac{\mathrm{d}\sigma}{\mathrm{d}\Omega} = \left(\frac{2Ze^2\csc^2(\theta/2)}{4E}\right)^2 \quad (5)$$

where Z is the atomic number of the scattering species, e is the elementary charge, θ is the scattering angle, and E is the energy of the incident particle. Here, the energy loss of the beam as it

Scheme 1. Formation of CPBs or Derivatized MLs Starting from Pristine ML-Br

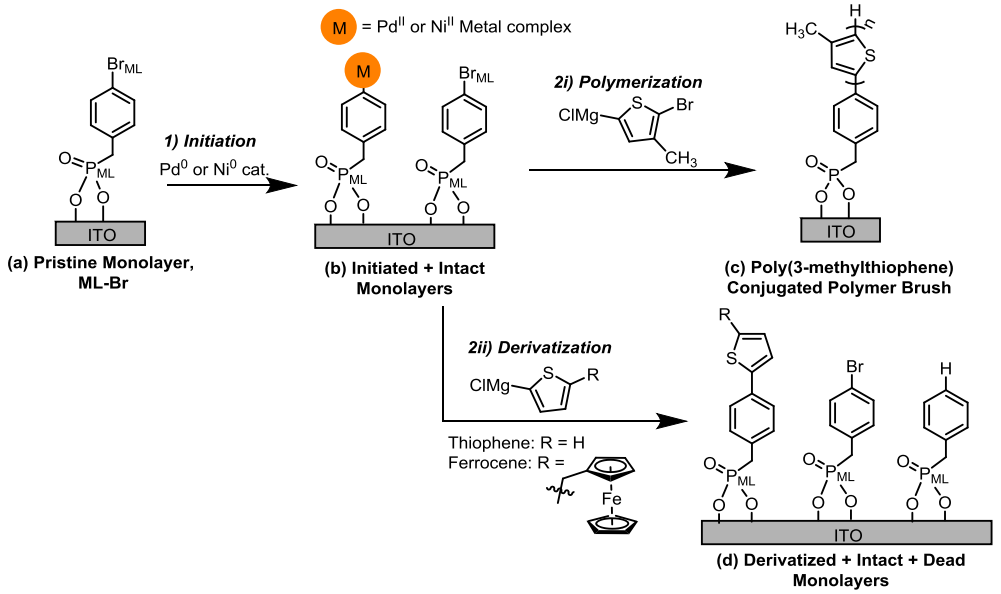

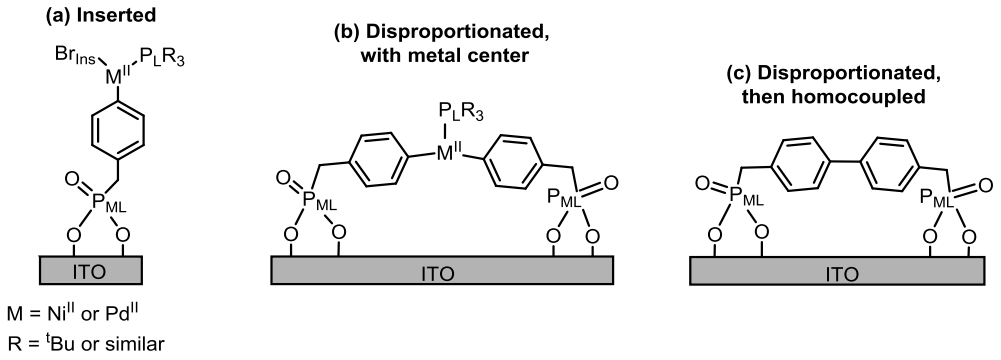

Figure 1. Proposed structures of initiated MLs formed from pristine **ML-Br**. P atoms from the phosphine ligand are labeled P_L to differentiate from phosphonate P_{ML} atoms.

travels through the polymer layer is negligible, so E is equal to the beam energy at the surface of the film and $d\sigma/d\Omega$ is constant throughout the film. $Q\Omega$ was determined from either the simulated or fit intensities of the known compositions of ITO (i.e., In and Sn contents) or the substrates (e.g., Si in glass or quartz) using eq 4.

The element of interest in the polymer films is S. In order to minimize background intensities and avoid convolutions of the S peak with other elements within the RBS spectra (specifically Si in the glass or quartz slides and impurities in the glass slides, such as Ca and Sb), different ITO slides were considered for the experiment and analysis, including several thicknesses of ITO and soda-lime glass versus fused quartz slides. We found that 60-nm-thick ITO on fused quartz was the optimal substrate for resolving and quantifying the S density in P3MT CPB and spun-cast P3HT films. This is because the ITO is thick enough for the S intensities to be separated from the onset of Si intensities from the substrate, and there are no detectable impurities in the vicinity of S intensities. If soda-lime glass slides had to be used, then the optimal ITO thickness was around 32 nm, where the S intensities lie between the onset of Ca impurity intensities and the onset of Si intensities (Figure S1).

RESULTS AND DISCUSSION

Aryl Halide Monolayer Initiation. This section describes the results from XPS experiments characterizing the structure and density of species formed during CPB growth. The XPS peak binding energies were used to identify changes in chemical structures, while the atomic ratios and signal intensities were used to qualitatively and quantitatively characterize the areal densities of surface chemical species.

Monolayer Synthesis and Characterization. Conjugated polymer brush (CPB) films composed of poly(3-methylthiophene) (P3MT) are typically grown using surface-initiated Kumada catalyst transfer polycondensation (SI-KCTP).[1,8,9,11] In SI-KCTP, as-grown aryl halide monolayers (MLs), referred to here as pristine MLs, are first initiated by a Pd^0 or Ni^0 catalyst with bulky phosphine ligands. The catalyst undergoes oxidative insertion to produce initiated MLs containing a three- or four-coordinate Pd^{II} or Ni^{II} complex (Scheme 1, step 1).

Halogenated aryl phosphonate monolayer **ML-Br** with the structure shown in Scheme 1a and Pd catalyst $Pd(P^tBu_3)_2$ were chosen to be used for this study because this monolayer/catalyst combination produces upon polymerization high-density CPB films with enhanced vertical polymer chain orientation.[1,9] The phosphonate-type P atom and aryl Br atom

present in pristine **ML-Br** are respectively labeled as P_{ML} and Br_{ML} in Scheme 1 and other chemical structures presented here. Potential chemical structures for initiated MLs (Scheme 1b) are described in detail below. XPS characterization of pristine **ML-Br** was consistent with its chemical structure (Figure S2).[8,31] These characteristics included an ~1:1 Br_{ML}/P_{ML} (Table S1, entry 1) atomic ratio and an ML density of 3.6 ± 0.1 nm^{-2} (calculated from intensities shown in Table S3, entry 1).

Initiation. As mentioned above, the chemical structures of species formed during the initiation of aryl halide MLs, here called initiated MLs, are not very well understood (Scheme 1b).[8,9] The chemical structures of initiated MLs are typically assumed to fall into two categories analogous to solution-phase initiation, shown in Figure 1: an inserted structure capable of mediating polymerization into CPBs upon introduction of a bifunctional monomer (Figure 1a) or disproportionated structures that are assumed to mediate homocoupling of the MLs instead of polymerization (Figure 1b,c).[8,9] Both the inserted and disproportionated structures are thought to contain a metal(II) center ligated by a phosphine ligand. Notably, the inserted and disproportionated chemical structures can be differentiated in XPS measurements by the halogen atom, which is present in the inserted structure (labeled Br_{Ins}) and is absent from the disproportionated and homocoupled structures.

Only one study has characterized aryl halide MLs initiated by a Ni catalyst,[7] and there are no reports characterizing MLs initiated by a Pd catalyst. In that study, the halogen XPS signal from the pristine ML was found to be at a higher binding energy before initiation. After initiation, a new halogen XPS peak appeared at a lower binding energy, indicating that a new initiated ML species was formed, which was assigned as an inserted structure analogous to Figure 1a.

In our case, after the initiation of pristine **ML-Br** with $Pd(P^tBu_3)_2$, a single Br 3d peak was detected at the same binding energy as before initiation, corresponding to Br_{ML} (Figure 2). The Br 3d peak also had a 60% lower intensity after initiation compared to the pristine ML (based on the Br_{ML}/P_{ML} atomic ratio, Table S1, entry 2). As expected, P_{ML} was detected after initiation with approximately the same intensity

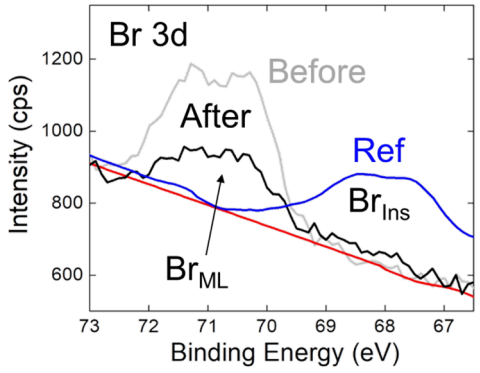

Figure 2. High-resolution XPS characterization of the Br 3d region in pristine **ML-Br** monolayers (gray trace), after initiation with $Pd(P^tBu_3)_2$ (black trace), and a reference catalyst with inserted structure (**ref**, blue trace; structure shown in Figure S4). Labels correspond to peak assignments to Br atoms in pristine **ML-Br** (Br_{ML}) or inserted ML (Br_{Ins}) structures. The background signal is shown by the red trace.

as in pristine **ML-Br** (based on the P_{ML}/substrate In atomic ratio) (Figure S3a). A new P peak at lower binding energy than for P_{ML} was also detected after initiation. The new peak was assigned to P atoms from the P^tBu_3 phosphine ligand (P_L), and had a P_L/P_{ML} atomic ratio of ~0.2. A complex Pd 3d XPS spectrum was detected after initiation, including at least three separate peaks with an overall Pd/P_{ML} atomic ratio of >1 and a P_L/Pd atomic ratio of ~0.1 (Figure S3b). The Pd peaks roughly correspond to Pd^0 and Pd^{II} species; however, we were not able to determine the exact number and structure of species.

These XPS results indicate that initiated MLs formed when pristine **ML-Br** is initiated by $Pd(P^tBu_3)_2$ do not have the expected inserted structure shown in Figure 1a because a new peak corresponding to Br_{Ins} (with a shifted binding energy compared to Br_{ML}) was not detected after initiation. To confirm the expected binding energy of Br_{Ins} compared to Br_{ML}, we recorded the Br 3d XPS spectrum from a commercially available reference catalyst that contained the inserted structure (ref, blue trace in Figure 2; structure in Figure S4). As expected, the Br 3d signal from Br_{Ins} in the reference catalyst was shifted to a lower binding energy compared to Br_{ML}.

These XPS results instead indicate that the initiated MLs formed using the Pd catalyst to initiate pristine **ML-Br** likely have one or both of the disproportionated structures shown in Figure 1b,c. On the basis of the decrease in the Br_{ML}/P_{ML} atomic ratio after initiation compared to before, disproportionated MLs account for ~60% of the ML after initiation. The remaining Br_{ML} signal detected after initiation likely comes from 40% of pristine MLs that were left intact during initiation (as shown in Scheme 1b). Intact MLs may remain after initiation because the Pd catalyst with bulky P^tBu_3 ligands is too large to initiate every aryl halide in the pristine ML film.

The complex, excess Pd signal detected after initiation has been observed previously[7] and likely arises from a mixture of disproportionated MLs containing a metal center (Figure 1b) and physisorbed Pd catalyst. The physisorbed catalyst results from the excess catalyst used during initiation, some of which "sticks" to the substrate/ML surface. Such physisorbed species were not able to be thoroughly cleaned off after the initiation step by sonication (as is typically done after CPB polymerization) without exposing the potentially air-sensitive initiated ML surface to the oxygen atmosphere. This assignment of Pd species is consistent with the formation of disproportionated MLs during initiation.

The intensity of P_L detected after initiation was lower than might be expected. The potential sources of Pd in the initiated samples (initiated MLs and physisorbed catalyst) were expected to contain a P_L/Pd atomic ratio of ~1, much higher than the observed P_L/Pd atomic ratio of ~0.1 (Table S1, entry 2). We offer three potential explanations for the unexpectedly low concentration of P_L: (1) some disproportionated MLs containing a metal center may undergo ligand exchange from the phosphine ligand to a solvent molecule during initiation, given the excess of solvents (THF and toluene) compared to phosphine ligands present during the initiation process; (2) some disproportionated MLs undergo homocoupling to form the structure shown in Figure 1c, which does not contain a metal center or a phosphine ligand (note that this explanation is discarded on the basis of the results below); and (3) the physisorbed catalyst molecules also undergo ligand exchange with the excess solvents and/or are partially composed of

Scheme 2. Proposed Derivatization Mechanism for ML-Br MLs Initiated by $Pd(P^tBu_3)_2$ and Then Derivatized with a Monofunctional Grignard Reagent

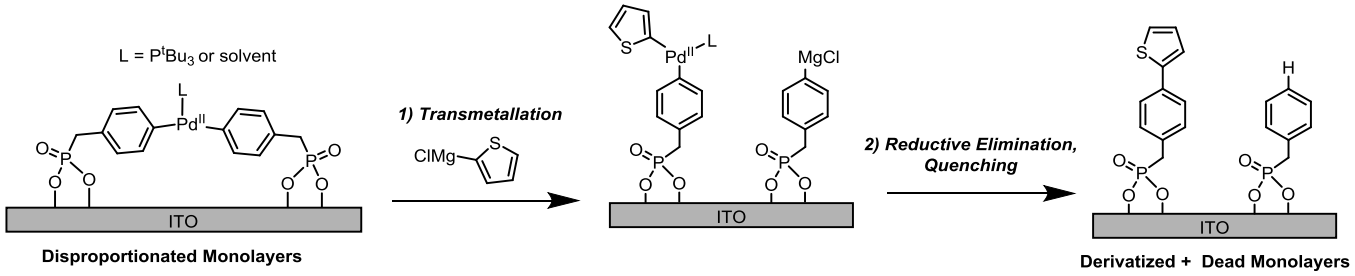

nonligated Pd, such as elemental Pd, a common impurity in commercially available Pd catalysts.[32] All three of these explanations would contribute to the observed reduction in the prevalence of the phosphine ligands after initiation.

Derivatization. After initiation, a bifunctional Grignard monomer is typically added to start polymerization that forms a CPB film (Scheme 1, step 2i). Alternatively, a monofunctional Grignard monomer with a quantifiable functional group can be added, derivatizing initiated MLs (Scheme 1, step 2ii). This derivatization step is useful in measuring the grafting density in CPB films, which is an important property of CPBs that determines the orientation and charge transport of polymer brushes.[9,10,33] The grafting density measured using derivatization should be treated as an upper bound because the calculation assumes that all derivatized MLs would polymerize into CPBs without premature termination. Note that the grafting density of CPB films cannot be directly measured after polymerization due to the insolubility of the P3MT polymer. A ferrocene-containing reagent has been used previously for derivatization, which can be quantified using oxidative cycling of the Fe center with cyclic voltammetry (CV).[8,9] However, a less bulky alternative to ferrocene derivatization is desirable to ensure that steric hindrance of the ferrocene derivatization reagent does not reduce the derivatization efficiency and apparent CPB grafting density.

Accordingly, we derivatized **ML-Br** initiated by $Pd(P^tBu_3)_2$ with monofunctional monomers functionalized with either ferrocene or thiophene. The density of these end groups was measured by either CV for ferrocene (measuring the density of the Fe metal center) or XPS for thiophene (measuring the density of the S atom), respectively (Figure S5a,b; quantitative XPS intensities shown in Table S3, entry 2). The density of derivatized MLs containing either end group was found to be nearly identical, either 1.3 nm^{-2} (ferrocene) or 1.2 ± 0.1 nm^{-2} (thiophene). These density values correspond to the grafting density of CPBs grown from **ML-Br** using $Pd(P^tBu_3)_2$).[9] Additionally, the density of intact MLs after derivatization was found to be 1.2 ± 0.1 nm^{-2} (Figure S5c), corresponding to an overall derivatization yield of 33% from pristine **ML-Br** (with a density of 3.6 nm^{-2}).

The most interesting implication of the initiation and derivatization results using $Pd(P^tBu_3)_2$ to initiate pristine **ML-Br** is that the disproportionated MLs formed during initiation can undergo derivatization or polymerization into CPBs. This further implies that the disproportionated MLs formed during initiation contain a metal center (Figure 1b), which would be required for a reaction with a Grignard reagent to occur. In other words, the homocoupled structure shown in Figure 1c was not formed here because it cannot undergo the derivatization that was observed. This result is distinct from studies that characterize the solution-phase initiation of aryl halides, which have shown that disproportionated species mediate homocoupling, not polymerization.[5,6] Scheme 2 shows a proposed mechanism for the derivatization of disproportionated MLs. In the scheme, half of the disproportionated MLs are derivatized while the other half become inert or dead MLs that are H-terminated (structure also shown in Scheme 1d). These ratios are consistent with our measured atomic densities: pristine **ML-Br** (3.6 nm^{-2}) is either left intact (1.2 nm^{-2}), forms derivatized MLs (1.2 nm^{-2}), or forms dead MLs (with the remaining 1.2 nm^{-2}).

Comparison of Monolayers and Catalysts. The surprising reactivity of disproportionated species demonstrated here may be specific to the initiation of surface-bound MLs or may be specific to the ML/catalyst combination of **ML-Br** and $Pd(P^tBu_3)_2$ used for initiation. To evaluate if the results are specific to the ML/catalyst combination, we repeated the initiation and derivatization experiments using $Pd(P^tBu_3)_2$ and Ni(dppp) (dppp = bis(diphenylphosphino)propane) to initiate pristine **ML-I**, which has the same structure as **ML-Br** except that an I atom substitutes for the Br atom (structure and characterization shown in Figures S6 and S7, respectively; quantitative XPS intensity shown in Table S3, entry 3).

We found that the initiation of **ML-I** with the Pd catalyst produced results identical to using **ML-Br**, indicating that initiation is not sensitive to the substitution of the halogen atom present in the ML (Figure S8 and Table S1, entry 4). Like the initiation of **ML-Br** or **ML-I** using the Pd catalyst, the initiation of **ML-I** by the Ni(dppp) catalyst also resulted in a decrease in the halogen I_{ML} signal compared to the pristine ML signal (Figure S9a,b; Table S1, entry 5). A new, shifted I 3d peak corresponding to I_{Ins} in an inserted structure was not detected after initiation. Thus, inserted MLs were not formed during the initiation of **ML-I** by the Ni catalyst; the XPS results are consistent with the formation of disproportionated MLs.

The derivatization of **ML-I** initiated by Ni(dppp) produced a much smaller grafting density (0.29 ± 0.04 nm^{-2}) than when the Pd catalyst was used (1.0 ± 0.1 nm^{-2}) (Figure S9c; Table S3, entries 4 and 5). This likely indicates that CPBs grown from **ML-I** or **ML-Br** using the $Pd(P^tBu_3)_2$ catalyst would have a higher grafting density and correspondingly more vertical orientation than CPBs grown using the Ni(dppp) catalyst, as suggested previously.[9] More interestingly, these results indicate a clear difference between disproportionated MLs formed after the initiation of **ML-Br** or **ML-I** by the Pd or Ni catalyst. Disproportionated MLs formed using the Pd catalyst can largely undergo derivatization or polymerization, while most of those formed using the Ni catalyst do not. This could be due to a difference in the stability of the disproportionated MLs containing a Ni or Pd center (Figure 1b). If a Ni center in the

structure is more reactive than a Pd center (as has been observed previously[34]), then the Ni center would be more likely than the Pd center to catalyze homocoupling (Figure 1c) before derivatization. An increase in homocoupling using the Ni catalyst would in turn produce more dead MLs and reduce the resulting grafting density compared to when the Pd catalyst was used, as we observed here.

Polymer Film Density. The surface morphology and polymer density in P3MT CPB and spun-cast poly(3-hexylthiophene) (P3HT) films were characterized using AFM and RBS techniques. The results for P3MT CPB films were compared to those of spun-cast P3HT because P3MT cannot be spun cast due to its insolubility, and spun-cast P3HT has been studied extensively.[35] However, P3HT CPBs cannot be grown from the ITO films and monolayers used here due to the steric hindrance of its long side chain.[36]

Film Synthesis and Surface Characterization. P3MT CPB films with thicknesses of 5−90 nm were grown by SI-KCTP from **ML-Br** monolayers using the $Pd(P^tBu_3)_2$ catalyst.[1,9] The CPB film thickness, as measured by AFM scratch profilometry, was controlled by the growth time. P3HT films with thicknesses of 8−200 nm were deposited via conventional spin casting. The dependence of film thickness and polymer areal density on growth time for P3MT CPB films is presented below.

In previous studies, P3MT CPBs were grown on 145-nm-thick ITO glass slides. However, the chemical composition and impurities in the glass slides (e.g., Si, Ca and K) and the thick ITO layer can interfere with the detection and quantification of S atoms by RBS. Therefore, CPB and spun-cast polymer films for RBS measurements were prepared on glass and quartz slides with 32- or 60-nm-thick ITO layers. The density and morphology of P3MT CPB and spun-cast P3HT films do not appear to be affected by the change in ITO thickness or the choice of glass or quartz slides. Specifically, the grafting density of P3MT CPB films grown on 60 nm ITO quartz slides was found to be 1.2 ± 0.2 nm^{-2} using the initiation/derivatization procedure described above, which is nearly identical to the value for P3MT CPB films grown on 145 nm ITO glass slides (Figure S10 and Table S3, entry 6). Additional evidence based on the characteristics of the polymer films' surface morphology and polymer density using AFM and RBS is described below.

The surface of P3MT CPB films grown on 60 nm ITO quartz exhibits columnar structures with characteristic cross-sectional dimensions and height distributions, as shown in the AFM topography image in Figure 3a. In contrast, spun-cast P3HT films are considerably smoother, without any characteristic structures or length scales (Figure 3b). The height distribution of the columns on the surface of the CPB films can be qualitatively represented by the histogram of surface height (Figure 3c). The surface height histograms of CPB films are very broad, with full width at half-maxima (fwhm) that are about half of the respective film thickness (Figure 3d). The CPB height histograms also exhibit a characteristic asymmetry such that the ratio of the right half-width at half-maximum (hwhm) to the left hwhm is approximately 1.2 (Figure 3e). These CPB surface characteristics from CPB samples grown on ITO quartz slides are identical to those observed in CPB films grown on 145 nm ITO glass slides, as reported previously.[1] The height distributions of spun-cast P3HT films shown in Figure 3c−e are narrow and symmetrical, with a surface roughness that does not change with film thickness.

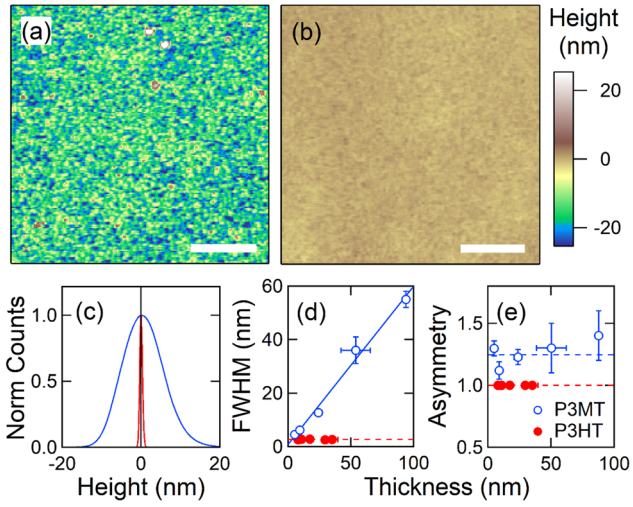

Figure 3. Comparison of AFM topography between P3MT CPB and spun-cast P3HT films. (a, b) AFM images of the P3MT CPB film (average thickness 24 ± 3 nm) and spun-cast P3HT film (average thickness 29 ± 1 nm), respectively. White scale bars are 1 μm. The height scale for (a) and (b) is shown to the right of (b). (c) Normalized histograms from (a) as a blue line with respective asymmetrical right and left hwhm values of 6.6 ± 0.1 and 5.7 ± 0.1 nm (fwhm of 12.3 ± 0.1 nm) and (b) as a red line with symmetrical left and right hwhm and a fwhm of 0.80 ± 0.01 nm. The maxima of both curves are centered at 0 nm height. (d, e) Thickness dependence of fwhm and width asymmetry (right/left hwhm), respectively. Points and error bars correspond respectively to the average value and standard deviation of ≥3 AFM profilometry and topography measurements. The solid line in (d) is a linear fit with a slope of 0.6 ± 0.1. The dashed lines in (d) and (e) are visual guides for constant behaviors.

RBS Characterization. RBS utilizes Coulomb scattering events to characterize the elemental composition and areal density in thin films as a function of depth.[29,30] The technique is widely used for studying the structural properties and compositions of inorganic and monolayer films, while there are only a handful of reports of its use in characterizing organic polymer films.[37−42] In principle, the technique is well-suited for characterizing the density of poly(3-alkylthiophene) (P3AT) polymer films because each monomer in the film contains a single sulfur atom which can be accurately quantified using RBS measurements and analysis.

Figure 4 shows representative RBS spectra and model simulations for P3MT CPB and spun-cast P3HT films on ITO quartz slides. Additional spectra for films on ITO glass slides are shown in Figure S1. Large backscattering intensities for In, Sn, Si, and O from the ITO quartz slides were detected at various energies (labeled in Figure 4a) and used in conjunction with the known composition of the ITO slides to determine the product of the cumulative incident particles and detector cross-section ($Q\Omega$ in eq 4). The small S peaks from the polymers were resolved at 1150−1300 keV. For polymer film samples on ITO glass slides, background signals in the energy region of interest for S correspond to those from Ca and Sb impurities in the glass (Figure S1), and they were estimated using either the simulation or the intensities determined from RBS measurements of the blank ITO glass slides. From the integrated intensity of the S peaks and the $Q\Omega$ values from In, Sn, or Si intensities, the S areal density for each polymer film sample was determined (eqs 4 and 5). The uncertainties

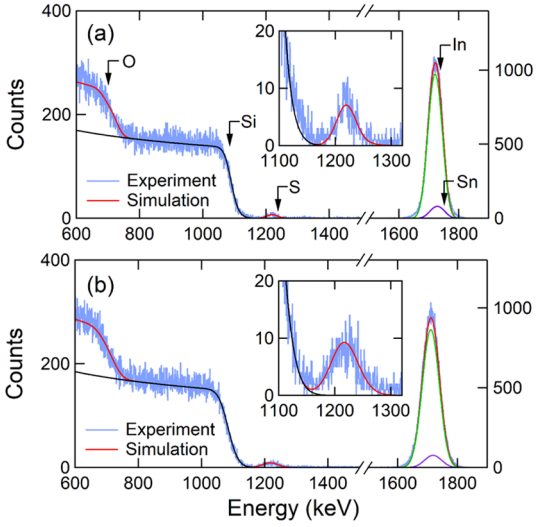

Figure 4. Typical experimental RBS spectra (blue) and model simulations (red) of (a) a P3MT CPB film (average thickness 24 ± 3 nm) and (b) a spun-cast P3HT film (average thickness 29 ± 1 nm) on 60 nm ITO quartz slides. The left (right) axes correspond to the respective spectra below (above) 1500 keV. Also shown are the contributions from several selected elements, including Si (black), In (green), and Sn (purple). The RBS onset energies of several elements are indicated by arrows in (a). Insets: expanded spectra in the vicinity of the polymer S intensities. Integrated intensities of the S peaks yield S areal densities of (a) 83 ± 9 and (b) 100 ± 10 atoms/nm^2.

associated with the S areal densities were estimated from the scatter within the S intensities to be ∼10−20 atoms/nm^2 for samples on ITO quartz slides and slightly higher for samples on ITO glass slides. As shown in the insets of Figures 4 and S1, there exists a small overlap between the intensities of Si and S, but our simulations show that the overlap is minimal and thus neglected in the results presented here.

We note that the P signal from the monolayer (∼1190 keV) and the Br signal (∼1630 keV) from the uninitiated/intact **ML-Br** monolayers or polymer chain ends were at least 1 order of magnitude below the detection limit of the experiment and thus undetectable. By and large, the simulations were modeled to accurately reproduce the measured spectra (Figures 4 and S1), with an exception for the tails of the In−Sn feature, where the model simulations tended to underestimate the measurements. The slightly enhanced scattering above the simulation is likely due to the heterogeneous thickness variation of the layers within the samples (especially P3MT CPB films), which was not modeled and considered negligible for estimating the $Q\Omega$ values.

The extent of high-energy ion beam damage in the polymer films was examined as a function of sample exposure. Polymer film samples were optically discolored after each RBS measurement, as evidently caused by the exposure to the high-energy ion beam (Figure S11a). In order to probe for any change in the elemental composition of the polymer film during an RBS measurement, the integrated S intensity was scaled by the integrated Si intensity (i.e., integrated intensity ratio of S/Si). The Si intensity was typically integrated between 800 and 1000 keV. This ratio was tracked as a function of the number of incident particles during the measurements (Figure S11b). The measured integrated S/Si ratios for P3MT CPB and spun-cast P3HT films do not show a significant decrease as the number of incident particles increases, indicating that the high-energy ion beam did not cause a significant change in the elemental composition of the films.

The areal density of S atoms (and thiophene monomers, by extension) in polymer films of different thicknesses was quantified using the RBS experiments and analysis described above (Figure 5). The measured areal densities for P3MT CPB

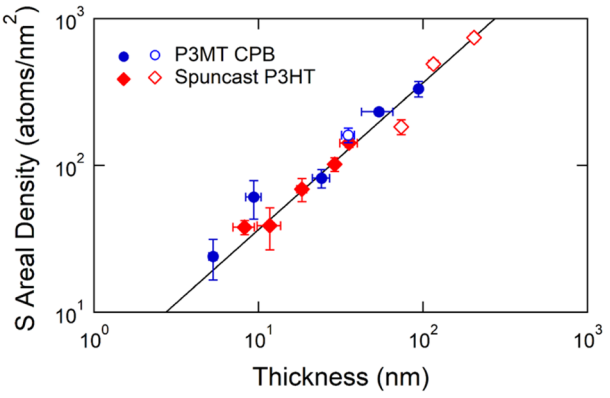

Figure 5. Areal density of S in P3MT CPB and spun-cast P3HT films as a function of film thickness. Closed (open) symbols correspond to films on 60 nm ITO quartz (32 nm ITO glass) slides. The error bars correspond to the standard deviation of the measurements. The line is a linear fit of all points with a slope of 3.7 ± 0.3 atoms/nm^3.

and spun-cast P3HT films exhibit a linear dependence on film thickness, spanning 2 orders of magnitude. The slope of the linear behavior for the two types of polymer films are indistinguishable from each other, with values of 3.9 ± 0.8 S atoms/nm^3 for the P3MT CPB films and 3.6 ± 0.4 S atoms/nm^3 for the spun-cast P3HT films. The slope can also be interpreted as a constant volume density that is independent of film thickness. In other words, the two types of polymer films have the same volume density of 3.7 ± 0.3 S atoms/nm^3 at all thicknesses (linear fit in Figure 5). This is qualitatively consistent with the previous observation in P3MT CPB films of surface topography consisting of columnar features with thickness-invariant length scales and shapes.[1] Note that the samples grown or spun cast on ITO glass slides (open symbols, Figure 5) follow the same trend as those on ITO quartz slides (closed symbols, Figure 5), indicating that the difference in substrate does not change the polymer density in the film.

P3MT and P3HT are known to potentially crystallize into different crystal structures with crystalline volume densities of 9.59 and 4.1−4.6 nm^{-3}, respectively.[1,43−47] Evidently, these densities are considerably higher than the volume densities reported here. This is quite reasonable because P3MT CPB and spun-cast P3HT films are known to exhibit low crystallinity.[1,46,47] The agreement in the volume density of P3MT CPB and spun-cast P3HT films suggests that low-crystallinity poly(3-alkylthiophene) films may adopt a characteristic volume density, despite their differences in side-chain length, deposition method, microstructure, and morphology. In contrast to the indistinguishable volume densities in the different film types, the calculated mass density of P3MT CPB films (0.59 ± 0.05 g/cm^{-3}) is much lower than that of spun-cast P3HT films (1.02 ± 0.08 g/cm^{-3}) owing to the much larger molecular weight of the 3-hexylthiophene monomer compared to the 3-methylthiophene monomer. Thus, we expect the grown P3MT CPB films to have more empty volume and porosity than spun-cast P3HT films.

CPB Growth and Orientation. The polymerization time dependence of P3MT CPB films was examined. Both the areal density of S atoms (i.e., the density of thiophene monomers) and the polymer film thickness exhibit linear dependences on the growth time, with respective slopes of 9 ± 1 S atoms/nm^2·h and 2.65 ± 0.02 nm/h (Figure 6). When combined with the

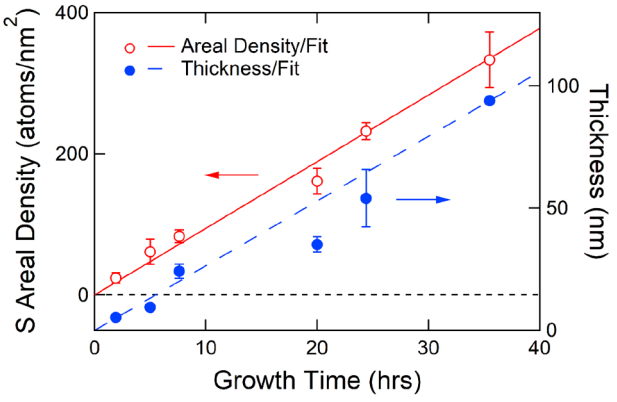

Figure 6. Polymerization time dependence of areal density and average film thickness in P3MT CPB films. The S areal density was determined by RBS experiments and analysis, while the film thickness was determined by AFM profilometry measurements. The lines are linear fits with slopes of 9 ± 1 S atoms/nm^2·h for the areal density (red) and 2.65 ± 0.02 nm/h for the thickness dependence (blue).

observed thickness-independent volume density, this result indicates that the thiophene monomers attach to the propagating chain ends at a constant rate during polymerization. The turnover frequency (i.e., monomer attachment rate) for P3MT CPB films was calculated to be 7.5 ± 0.8 h^{-1} per chain, using the measured slope of areal density versus time and the measured polymer grafting density. We note that since the areal density and film thickness were measured by independent means, the fact that they show a linear dependence on each other in Figure 5 provides additional credence for the reliability of the growth-time-dependent result presented here.

The average thickness-independent degree of polymerization (3.1 ± 0.8 nm^{-1}) and molecular weight (300 ± 70 g/mol·nm) in P3MT CPBs were calculated from the volume density and grafting density values reported above (P3MT monomer molecular weight = 96.15 g/mol). Using the degree of polymerization and the repeat unit distance in polypolythiophenes of 0.39 nm,[45] an estimated ensemble average tilt angle of 34° from the normal was calculated for P3MT CPB films of all thicknesses. This tilt angle is well below the isotropic tilt angle of 54.7°, indicating modest vertical orientation in P3MT CPBs. This is consistent with the mild vertical orientation measured in P3MT CPB films using polarized oblique UV−vis spectroscopy.[1] These parameters were determined under the assumption that all initiated monolayers grow into polymer chains. Premature termination has been observed in SI-KCTP,[1,48] so the effective grafting density in P3MT CPB films as they polymerize may be lower than what is reported here. Thus, the calculated values of the degree of polymerization and molecular weight in P3MT CPB films are lower bounds, while the ensemble-average tilt angle is an upper bound.

CONCLUSIONS

We report the characterization of initiation and polymer density in conjugated polymer brushes (CPBs). Using X-ray photoelectron spectroscopy, we found that disproportionated monolayers are formed during the initiation of aryl halide monolayers with Pd or Ni catalysts and that those formed using the Pd catalyst were more viable for derivatization or polymerization than those formed using the Ni catalyst. This result is a marked difference from disproportionated species formed during the solution-phase initiation of aryl halides, which are generally unable to undergo polymerization. Using RBS, we found that the volume densities of conjugated polymer brush films and the analogous spun-cast films do not change with thickness and have the same value. The volume density value of CPB films was combined with the measured initiation and growth parameters to determine the turnover frequency and molecular weight of CPB films for the first time. The ensemble average tilt angle calculated from the degree of polymerization indicates net vertical orientation in the CPB films, consistent with previous reports. These results greatly improve our understanding of the growth mechanism and morphology in CPB films and showcase the value of the RBS technique for characterizing polymer films, especially for films composed of insoluble polymers such as P3MT. Finally, the methods employed in this work can be used to study the relationships between synthetic parameters used to grow CPBs and their resulting properties (i.e., these methods are generally applicable to comparing the properties of CPB films that are grown using different monolayers, catalysts, or monomers to the model system presented here).

ASSOCIATED CONTENT

Supporting Information

The Supporting Information is available free of charge at https://pubs.acs.org/doi/10.1021/acs.jpcb.0c06923.

Additional tables and figures related to X-ray photoelectron constants, spectra, peak energies, and peak intensities; Rutherford backscattering spectrometry spectra, simulations, and beam damage; cyclic voltammograms; and key chemical structures (PDF)

AUTHOR INFORMATION

Corresponding Authors

Frank Tsui − *Department of Physics and Astronomy, University of North Carolina at Chapel Hill, Chapel Hill, North Carolina 27599, United States*; Email: ftsui@physics.unc.edu

Wei You − *Department of Chemistry, University of North Carolina at Chapel Hill, Chapel Hill, North Carolina 27599, United States*; orcid.org/0000-0003-0354-1948; Email: wyou@unc.edu

Authors

Ian A. VonWald − *Department of Chemistry, University of North Carolina at Chapel Hill, Chapel Hill, North Carolina 27599, United States*; orcid.org/0000-0001-9575-1840

S. Gaither Frye − *Department of Physics and Astronomy, University of North Carolina at Chapel Hill, Chapel Hill, North Carolina 27599, United States*

Mark M. Moog − *Department of Physics and Astronomy, University of North Carolina at Chapel Hill, Chapel Hill, North Carolina 27599, United States*

Carrie L. Donley − *Department of Applied Physical Sciences, University of North Carolina at Chapel Hill, Chapel Hill, North Carolina 27599, United States;* orcid.org/0000-0003-0906-306X

Complete contact information is available at: https://pubs.acs.org/10.1021/acs.jpcb.0c06923

Notes

The authors declare no competing financial interest.

■ ACKNOWLEDGMENTS

The authors acknowledge the following support for this collaborative research. I.A.V.W. was supported by a National Science Foundation Graduate Research Fellowship under grant no. DGE-1650116. W.Y. was supported by NSF grant nos. CHE-1412286 and DMR-1610879. F.T. and S.G.F. were supported by NSF grant no. DMR-1905651. Parts of this work were performed in part at the Chapel Hill Analytical and Nanofabrication Laboratory, CHANL, a member of the North Carolina Research Triangle Nanotechnology Network, RTNN, which is supported by the National Science Foundation, grant ECCS-1542015, as part of the National Nanotechnology Coordinated Infrastructure, NNCI. The use of the Tandem beamline at the Triangle Universities Nuclear Laboratories (TUNL) was supported in part by the U.S. Department of Energy, Office of Nuclear Physics, grant numbers 97ER41041 and 97ER41033. The authors thank Richard Longland, Tom Clegg, and Hugon Karwowski for assistance with the RBS experiments and Nalin Parikh for RBS analysis. The authors thank Brett Bowman for the synthesis of the P3MT monomer.

■ REFERENCES

(1) Vonwald, I. A.; Moog, M. M.; Lajoie, T. W.; Yablonski, J. D.; Delongchamp, D. M.; Locklin, J.; Tsui, F.; You, W. Morphology, Structure, and Enhanced Intramolecular Conduction in Ultralong Conjugated Polymer Brushes. *J. Phys. Chem. C* **2018**, *122* (14), 7586−7596.

(2) Roy, A.; Bougher, T. L.; Geng, R.; Ke, Y.; Locklin, J.; Cola, B. A. Thermal Conductance of Poly(3-Methylthiophene) Brushes. *ACS Appl. Mater. Interfaces* **2016**, *8* (38), 25578−25585.

(3) Geng, R.; Roy, A.; Zhao, W.; Subedi, R. C.; Li, X.; Locklin, J.; Nguyen, T. D. Engineering of Spin Injection and Spin Transport in Organic Spin Valves Using π-Conjugated Polymer Brushes. *Adv. Funct. Mater.* **2016**, *26* (22), 3999−4006.

(4) Yang, L.; Sontag, S. K.; LaJoie, T. W.; Li, W.; Huddleston, N. E.; Locklin, J.; You, W. Surface-Initiated Poly(3-Methylthiophene) as a Hole-Transport Layer for Polymer Solar Cells with High Performance. *ACS Appl. Mater. Interfaces* **2012**, *4* (10), 5069−5073.

(5) Bronstein, H. A.; Luscombe, C. K. Externally Initiated Regioregular P3HT with Controlled Molecular Weight and Narrow Polydispersity. *J. Am. Chem. Soc.* **2009**, *131* (36), 12894−12895.

(6) Stambuli, J. P.; Incarvito, C. D.; Bühl, M.; Hartwig, J. F. Synthesis, Structure, Theoretical Studies, and Ligand Exchange Reactions of Monomeric, T-Shaped Arylpalladium(II) Halide Complexes with an Additional, Weak Agostic Interaction. *J. Am. Chem. Soc.* **2004**, *126* (4), 1184−1194.

(7) Youm, S. G.; Hwang, E.; Chavez, C. A.; Li, X.; Chatterjee, S.; Lusker, K. L.; Lu, L.; Strzalka, J.; Ankner, J. F.; Losovyj, Y.; et al. Polythiophene Thin Films by Surface-Initiated Polymerization: Mechanistic and Structural Studies. *Chem. Mater.* **2016**, *28* (13), 4787−4804.

(8) Sontag, S. K.; Sheppard, G. R.; Usselman, N. M.; Marshall, N.; Locklin, J. Surface-Confined Nickel Mediated Cross-Coupling Reactions: Characterization of Initiator Environment in Kumada Catalyst-Transfer Polycondensation. *Langmuir* **2011**, *27* (19), 12033−12041.

(9) Huddleston, N. E.; Sontag, S. K.; Bilbrey, J. A.; Sheppard, G. R.; Locklin, J. Palladium-Mediated Surface-Initiated Kumada Catalyst Polycondensation: A Facile Route Towards Oriented Conjugated Polymers. *Macromol. Rapid Commun.* **2012**, *33* (24), 2115−2120.

(10) Wu, T.; Efimenko, K.; Vleek, P.; Šubr, V.; Genzer, J. Formation and Properties of Anchored Polymers with a Gradual Variation of Grafting Densities on Flat Substrates. *Macromolecules* **2003**, *36* (7), 2448−2453.

(11) Doubina, N.; Jenkins, J. L.; Paniagua, S. A.; Mazzio, K. A.; MacDonald, G. A.; Jen, A. K.-Y.; Armstrong, N. R.; Marder, S. R.; Luscombe, C. K. Surface-Initiated Synthesis of Poly(3-Methylthiophene) from Indium Tin Oxide and Its Electrochemical Properties. *Langmuir* **2012**, *28* (3), 1900−1908.

(12) Zhugayevych, A.; Mazaleva, O.; Naumov, A.; Tretiak, S. Lowest-Energy Crystalline Polymorphs of P3HT. *J. Phys. Chem. C* **2018**, *122* (16), 9141−9151.

(13) Kline, R. J.; McGehee, M. D. Morphology and Charge Transport in Conjugated Polymers. *J. Macromol. Sci., Polym. Rev.* **2006**, *46* (1), 27−45.

(14) Coropceanu, V.; Cornil, J.; da Silva Filho, D. A.; Olivier, Y.; Silbey, R.; Brédas, J. L. Charge Transport in Organic Semiconductors. *Chem. Rev.* **2007**, *107* (4), 926−952.

(15) Trznadel, M.; Pron, a; Zagorska, M.; Chrzaszcz, R.; Pielichowski, J. Effect of Molecular Weight on Spectroscopic and Spectroelectrochemical Properties of Regioregular Poly(3-Hexylthiophene). *Macromolecules* **1998**, *31* (15), 5051−5058.

(16) Himmelberger, S.; Vandewal, K.; Fei, Z.; Heeney, M.; Salleo, A. Role of Molecular Weight Distribution on Charge Transport in Semiconducting Polymers. *Macromolecules* **2014**, *47* (20), 7151−7157.

(17) Elgrishi, N.; Rountree, K. J.; McCarthy, B. D.; Rountree, E. S.; Eisenhart, T. T.; Dempsey, J. L. A Practical Beginner's Guide to Cyclic Voltammetry. *J. Chem. Educ.* **2018**, *95* (2), 197−206.

(18) Moulder, J. F., Stickle, W. F.; Sobol, P. E.; Bonben, K. D. *Handbook of X-ray Photoelectron Spectroscopy*; Chastain, J., Ed.; Perkin-Elmer Corporation: Eden Prairie, MN, 1992.

(19) Demissie, A. T.; Haugstad, G.; Frisbie, C. D. Growth of Thin, Anisotropic, π-Conjugated Molecular Films by Stepwise "Click" Assembly of Molecular Building Blocks: Characterizing Reaction Yield, Surface Coverage, and Film Thickness versus Addition Step Number. *J. Am. Chem. Soc.* **2015**, *137* (27), 8819−8828.

(20) Powell, C. J.; Jablonski, A. Progress in Quantitative Surface Analysis by X-Ray Photoelectron Spectroscopy: Current Status and Perspectives. *J. Electron Spectrosc. Relat. Phenom.* **2010**, *178−179* (C), 331−346.

(21) Powell, C. J.; Werner, W. S. M.; Smekal, W. Effects of Elastic Scattering and Analyzer-Acceptance Angle on the Analysis of Angle-Resolved X-Ray Photoelectron Spectroscopy Data. *Surf. Interface Anal.* **2011**, *43* (7), 1046−1056.

(22) Scofield, J. H. Hartree-Slater Subshell Photoionization Cross-Sections at 1254 and 1487 EV. *J. Electron Spectrosc. Relat. Phenom.* **1976**, *8* (2), 129−137.

(23) Jablonski, A. Database of Correction Parameters for the Elastic Scattering Effects in XPS. *Surf. Interface Anal.* **1995**, *23* (1), 29−37.

(24) Reilman, R. F.; Msezane, A.; Manson, S. T. Relative Intensities in Photoelectron Spectroscopy of Atoms and Molecules. *J. Electron Spectrosc. Relat. Phenom.* **1976**, *8* (5), 389−394.

(25) Yarzhemsky, V. G.; Nefedov, V. I.; Trzhaskovskaya, M. B.; Band, I. M.; Szargan, R. The Influence of Core Hole Relaxation on the Main-Line Intensities in X-Ray Photoelectron Spectra. *J. Electron Spectrosc. Relat. Phenom.* **2002**, *123* (1), 1−10.

(26) Cumpson, P. J.; Seah, M. P. Elastic Scattering Corrections in AES and XPS. II. Estimating Attenuation Lengths and Conditions Required for Their Valid Use in Overlayer/Substrate Experiments. *Surf. Interface Anal.* **1997**, *25* (6), 430−446.

(27) Tanuma, S.; Powell, C. J.; Penn, D. R. Calculations of Electron Inelastic Mean Free Paths. *Surf. Interface Anal.* **2005**, *37* (1), 1−14.

(28) Powell, C. J.; Jablonski, A. Evaluation of Calculated and Measured Electron Inelastic Mean Free Paths Near Solid Surfaces. *J. Phys. Chem. Ref. Data* **1999**, *28* (1), 19−62.
(29) Chu, W.-K.; Mayer, J. W.; Nicolet, M. A. *Backscattering Spectrometry*; Elsevier: Amsterdam, 1978.
(30) Jeynes, C.; Barradas, N. P.; Szilágyi, E. Accurate Determination of Quantity of Material in Thin Films by Rutherford Backscattering Spectrometry. *Anal. Chem.* **2012**, *84* (14), 6061−6069.
(31) Hanson, E. L.; Schwartz, J.; Nickel, B.; Koch, N.; Danisman, M. F. Bonding Self-Assembled, Compact Organophosphonate Monolayers to the Native Oxide Surface of Silicon. *J. Am. Chem. Soc.* **2003**, *125* (51), 16074−16080.
(32) Zalesskiy, S. S.; Ananikov, V. P. Pd 2 Dba 3 as a Precursor of Soluble Metal Complexes and Nanoparticles: Determination of Pd Active Species for Catalysis and Synthesis. *Organometallics* **2012**, *6* (499), 2302−12309.
(33) Liu, G.; Yan, L.; Chen, X.; Zhang, G. Study of the Kinetics of Mushroom-to-Brush Transition of Charged Polymer Chains. *Polymer* **2006**, *47* (9), 3157−3163.
(34) Balcells, D.; Nova, A. Designing Pd and Ni Catalysts for Cross-Coupling Reactions by Minimizing Off-Cycle Species. *ACS Catal.* **2018**, *8* (4), 3499−3515.
(35) DeLongchamp, D. M.; Kline, R. J.; Fischer, D. A.; Richter, L. J.; Toney, M. F. Molecular Characterization of Organic Electronic Films. *Adv. Mater.* **2011**, *23* (3), 319−337.
(36) Marshall, N.; Sontag, S. K.; Locklin, J. Substituted Poly(p-Phenylene) Thin Films via Surface-Initiated Kumada-Type Catalyst Transfer Polycondensation. *Macromolecules* **2010**, *43* (5), 2137−2144.
(37) Khanduyeva, N.; Senkovskyy, V.; Beryozkina, T.; Bocharova, V.; Simon, F.; Nitschke, M.; Stamm, M.; Grötzschel, R.; Kiriy, A. Grafting of Poly(3-Hexylthiophene) from Poly(4-Bromostyrene) Films by Kumada Catalyst-Transfer Polycondensation: Revealing of the Composite Films Structure. *Macromolecules* **2008**, *41* (20), 7383−7389.
(38) Goffri, S.; Müller, C.; Stingelin-Stutzmann, N.; Breiby, D. W.; Radano, C. P.; Andreasen, J. W.; Thompson, R.; Janssen, R. a J.; Nielsen, M. M.; Smith, P.; et al. Multicomponent Semiconducting Polymer Systems with Low Crystallization-Induced Percolation Threshold. *Nat. Mater.* **2006**, *5* (December), 950−956.
(39) Erwin, M. M.; McBride, J.; Kadavanich, A. V.; Rosenthal, S. J. Effects of Impurities on the Optical Properties of Poly-3-Hexylthiophene Thin Films. *Thin Solid Films* **2002**, *409* (2), 198−205.
(40) Urien, M.; Wantz, G.; Cloutet, E.; Hirsch, L.; Tardy, P.; Vignau, L.; Cramail, H.; Parneix, J.-P. Field-Effect Transistors Based on Poly(3-Hexylthiophene): Effect of Impurities. *Org. Electron.* **2007**, *8* (6), 727−734.
(41) Zhang, Y.; Parnell, A. J.; Pontecchiani, F.; Cooper, J. F. K.; Thompson, R. L.; Jones, R. A. L.; King, S. M.; Lidzey, D. G.; Bernardo, G. Understanding and Controlling Morphology Evolution via DIO Plasticization in PffBT4T-2OD/PC 71 BM Devices. *Sci. Rep.* **2017**, *7* (July 2016), 44269.
(42) de Jong, M. P.; van IJzendoorn, L. J.; de Voigt, M. J. A. Stability of the Interface between Indium-Tin-Oxide and Poly(3,4-Ethylenedioxythiophene)/Poly(Styrenesulfonate) in Polymer Light-Emitting Diodes. *Appl. Phys. Lett.* **2000**, *77* (14), 2255−2257.
(43) Yamamoto, T.; Komarudin, D.; Arai, M.; Lee, B.-L.; Suganuma, H.; Asakawa, N.; Inoue, Y.; Kubota, K.; Sasaki, S.; Fukuda, T.; et al. Extensive Studies on π-Stacking of Poly(3-Alkylthiophene-2,5-Diyl)s and Poly(4-Alkylthiazole-2,5-Diyl)s by Optical Spectroscopy, NMR Analysis, Light Scattering Analysis, and X-Ray Crystallography. *J. Am. Chem. Soc.* **1998**, *120* (9), 2047−2058.
(44) Hou, W.; Zhao, N. J.; Meng, D.; Tang, J.; Zeng, Y.; Wu, Y.; Weng, Y.; Cheng, C.; Xu, X.; Li, Y.; et al. Controlled Growth of Well-Defined Conjugated Polymers from the Surfaces of Multiwalled Carbon Nanotubes: Photoresponse Enhancement via Charge Separation. *ACS Nano* **2016**, *10* (5), 5189−5198.
(45) Kayunkid, N.; Uttiya, S.; Brinkmann, M. Structural Model of Regioregular Poly(3-Hexylthiophene) Obtained by Electron Diffraction Analysis. *Macromolecules* **2010**, *43* (11), 4961−4967.
(46) Kohn, P.; Rong, Z.; Scherer, K. H.; Sepe, A.; Sommer, M.; Müller-Buschbaum, P.; Friend, R. H.; Steiner, U.; Hüttner, S. Crystallization-Induced 10-Nm Structure Formation in P3HT/PCBM Blends. *Macromolecules* **2013**, *46* (10), 4002−4013.
(47) Shen, X.; Hu, W.; Russell, T. P. Measuring the Degree of Crystallinity in Semicrystalline Regioregular Poly(3-Hexylthiophene). *Macromolecules* **2016**, *49* (12), 4501−4509.
(48) Marshall, N.; Rodriguez, A. Cross-Coupling Polymerization at Iodophenyl Thin Films Prepared by Spontaneous Grafting of a Diazonium Salt. *PeerJ. Mater. Sci.* **2020**, *2*, No. e6.